

Phosphane-free C–C Heck couplings catalyzed by Pd(II) fluorinated aniline complexes of the type *trans*-[PdCl₂(NH₂Ar^F)₂]

Oscar Baldovino-Pantaleón, Joaquín Barroso-Flores, J.A. Cogordan¹,
Simón Hernández-Ortega, Rubén A. Toscano, David Morales-Morales*

Instituto de Química, Universidad Nacional Autónoma de México, Cd. Universitaria, Circuito Exterior Coyoacán, 04510 México, D.F., México

Received 4 October 2005; received in revised form 15 November 2005; accepted 15 November 2005

Available online 27 December 2005

Abstract

A series of palladium fluoro-aniline complexes of the *trans*-[PdCl₂(NH₂Ar^F)₂] type were synthesized in good yields by direct reaction of *trans*-[PdCl₂(C₆H₅CN)] with Ar^FNH₂; Ar^F = C₆H₃-2,3-F₂ (**1**), C₆H₃-2,5-F₂ (**2**), C₆H₃-3,4-F₂ (**3**), C₆H₃-3,5-F₂ (**4**), C₆H₂-2,3,4-F₃ (**5**), C₆H₂-2,3,6-F₃ (**6**), C₆H₂-2,4,5-F₃ (**7**), C₆H₂-2,4,6-F₃ (**8**), C₆F₄-4-H (**9**), C₆F₅ (**10**). The crystal structures of complexes **3**, **4** and **5** were determined. Heck coupling reactions were carried out using complexes 1–10 as catalysts in order to examine the effect of the fluorinated anilines in the reaction of bromobenzene and styrene.

© 2005 Elsevier B.V. All rights reserved.

Keywords: Aniline ligands; Fluorinated amines; Heck reaction; C–C coupling reactions; Fluorinated amine complexes; Palladium complexes; Crystal structures; Catalysis

1. Introduction

Palladium catalyzed C–C coupling reactions have been recognized as power tools in multiple organic transformations, from these the Heck reaction has become a corner stone in modern organic synthesis [1]. This reaction consists in the coupling of a halo compound with an alkene. The importance of this reaction has transcended its applications in the laboratory and become of main interest at the industrial level [2]. The different catalysts employed to carry out this reaction have also evolved to achieve a better understanding of the factors that influence activity, selectivity and stability. Thus, in recent years, several groups have been involved in the design of ligands able to tolerate an oxidizing atmosphere, allowing Heck couplings in a more efficient manner employing cheap reagent grade starting materials. The use of cheap, easy to synthesize catalysts such that the synthesis of the catalyst will not represent a challenge but an advantage has become a main research challenge. Thus, given our continuous interest in the design and synthesis

of active complexes as potential catalysts in industrial relevant transformations [3], we report here our findings in the use of a very simple, easy to synthesize series of complexes of the type *trans*-[PdCl₂(NH₂Ar^F)₂] based on fluorinated anilines for the potential tuning of the electronics. The identification of the electronic effects of the different fluorinated aniline palladium complexes over the reactivity of these palladium complexes in the Heck catalytic reaction of bromobenzene and styrene will be discussed.

2. Experimental

2.1. Materials and methods

Unless stated otherwise, all reactions were carried out under an atmosphere of dinitrogen using conventional Schlenk glassware. Solvents were dried using established procedures and distilled under dinitrogen immediately prior to use. The IR spectra were recorded on a Nicolet-Magna 750 FT-IR spectrometer as KBr pellets. The ¹H NMR (300 MHz) spectra were recorded on a JEOL GX300 spectrometer. Chemical shifts are reported in ppm down field of TMS using the solvent (CDCl₃) as an internal standard. ¹⁹F{¹H} spectra were recorded with proton decoupling and are reported in ppm using C₆F₆ as external standard.

* Corresponding author. Tel.: +52 555 622 4514; fax: +52 555 616 2217.

E-mail addresses: cogordan@servidor.unam.mx (J.A. Cogordan), damor@servidor.unam.mx (D. Morales-Morales).

¹ J.A. Cogordan is responsible for the theoretical calculations.

Elemental analyses were determined on a Perkin-Elmer 240. Positive-ion FAB mass spectra were recorded on a JEOL JMS-SX102A mass spectrometer operated at an accelerating voltage of 10 kV. Samples were desorbed from a nitrobenzyl alcohol (NBA) matrix using 3 keV xenon atoms. Mass measurements in FAB are performed at a resolution of 3000 using magnetic field scans and the matrix ions as the reference material or, alternatively, by electric field scans with the sample peak bracketed by two (polyethylene glycol or cesium iodide) reference ions. GC–MS analyses were performed on an Agilent 6890N GC with a 30.0 m DB-1MS capillary column coupled to an Agilent 5973 Inert Mass Selective detector. Melting points were determined in a MEL-TEMP capillary melting point apparatus and are reported without correction.

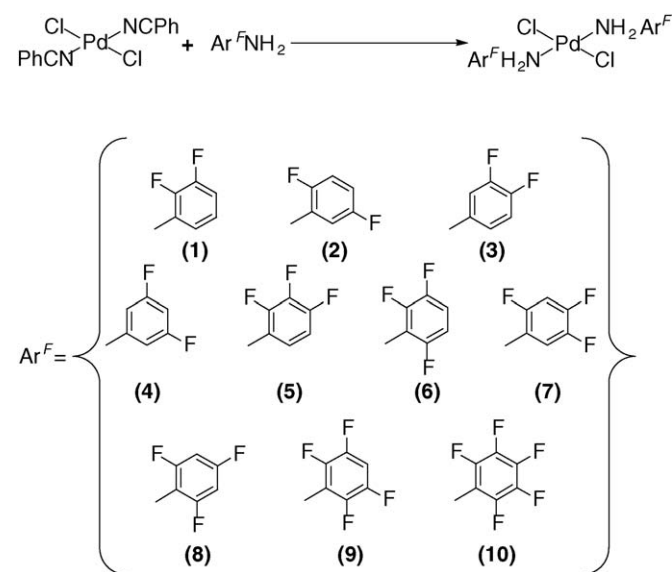
PdCl_2 and fluorinated anilines were obtained commercially from Aldrich Chem. Co. Compound *trans*- $[\text{PdCl}_2(\text{C}_6\text{H}_5\text{CN})]$ [4], was synthesized according to the published procedures.

2.2. General procedure for the synthesis of the complexes *trans*- $[\text{PdCl}_2(\text{NH}_2\text{Ar}^F)_2]$

All the complexes were obtained using the same experimental procedure. As a representative example, the synthesis of *trans*- $[\text{Pd}(\text{Cl})_2(\text{NH}_2\text{C}_6\text{H}_4-2,3-\text{F}_2)_2]$ (**1**) is described (Scheme 1).

2.2.1. Synthesis of *trans*- $[\text{Pd}(\text{Cl})_2(\text{NH}_2\text{C}_6\text{H}_3-2,3-\text{F}_2)_2]$ (**1**)

A solution, 15 mL ethanol of $[\text{PdCl}_2(\text{C}_6\text{H}_5\text{CN})]$ (100 mg, 0.26 mmol, 1 equiv) was added to a 15 mL ethanol solution with 68 mg (0.52 mmol, 2.0 equiv) of 2,3-fluoroaniline. The mixture was reflux 8 h. After this time, the hot solution was filtrated and the solvent removed under *vacuum*. Yellow crystalline powder was obtained in good yield. The single crystals suitable for X-ray diffraction studies were obtained from CH_2Cl_2 –MeOH (1:1) solution. Yellow solid, yield 98 mg (87%), mp 215–217 °C. ^1H NMR (DMSO- d_6): δ 6.82 (dd, $^3J=7.7$ Hz, 2H, H_6), 6.54 (t,



Scheme 1. Reactions for the synthesis of the complexes *trans*- $[\text{PdCl}_2(\text{NH}_2\text{Ar}^F)_2]$.

$^3J=8.25$, 7.7 Hz, 2H, H_5), 6.45 (dd, $J=8.25$ Hz, 2H, H_4), 5.46 (br, 4H, N–H). $^{19}\text{F}\{^1\text{H}\}$ NMR (DMSO- d_6): δ –141.20 (m, F_2), –162.52 (m, F_3). FT-IR (KBr, cm^{-1}): ν (N–H) 3250.50(m), 3167.40(m), 3100.69(s), δ (N–H) 1577.38(m), 1510.63(s). MS-FAB $^+$: m/z 436 (M^+ , 2%). Elemental analysis calculated for $[\text{C}_{12}\text{H}_{10}\text{F}_4\text{N}_2\text{Cl}_2\text{Pd}]$ calcd. %: C, 33.09; H, 2.31; found C, 34.08; H, 2.38.

2.2.2. Synthesis of *trans*- $[\text{Pd}(\text{Cl})_2(\text{NH}_2\text{C}_6\text{H}_3-2,5-\text{F}_2)_2]$ (**2**)

Yellow solid, yield 106 mg (93.3%), mp 215–217 °C. ^1H NMR (DMSO- d_6): δ 6.97 (m, 2H, H_6), 6.50 (m, 2H, H_4), 6.25 (m, 2H, H_3), 5.46 (br, 4H, N–H); $^{19}\text{F}\{^1\text{H}\}$ NMR (DMSO- d_6): δ –119.45 (m, F_5), –141.29 (m, F_2). FT-IR (KBr, cm^{-1}): ν (N–H) 3237.45(m), 3177.10(m), 3102.41(m); δ (N–H) 1576.70(m), 1510.24(s). MS-FAB $^+$: m/z 436(M^+ , 7%). Elemental analysis for $[\text{C}_{12}\text{H}_{10}\text{F}_4\text{N}_2\text{Cl}_2\text{Pd}]$ calcd. %: C, 33.09; H, 2.31; found C, 32.43; H, 2.38.

2.2.3. Synthesis of *trans*- $[\text{Pd}(\text{Cl})_2(\text{NH}_2\text{C}_6\text{H}_3-3,4-\text{F}_2)_2]$ (**3**)

Yellow solid, yield 93.3 mg (83.7%); mp 297–299 °C. ^1H NMR (DMSO- d_6): δ 7.35–7.20 (m, 2H, H_2), 7.06 (m, 2H, H_6), 6.45–6.29 (m, 2H, H_3), 5.24 (br, 4H, N–H); $^{19}\text{F}\{^1\text{H}\}$ NMR (DMSO- d_6): δ –139.65 (m, F_4), –156.63 (m, F_3). FT-IR (KBr, cm^{-1}): ν (N–H) 3289.59(m), 3203.72(s), 3116.51(m), δ (N–H) 1569.32(m), 1520.91(s). MS-FAB $^+$: m/z 436 (M^+ , 10%). Elemental analysis for $[\text{C}_{12}\text{H}_{10}\text{F}_4\text{N}_2\text{Cl}_2\text{Pd}]$ calcd. %: C, 33.09; H, 2.31; found C, 33.92; H, 2.37.

2.2.4. Synthesis of *trans*- $[\text{Pd}(\text{Cl})_2(\text{NH}_2\text{C}_6\text{H}_3-3,5-\text{F}_2)_2]$ (**4**)

Yellow solid, yield 100 mg (88%), mp 305–307 °C. ^1H NMR (DMSO- d_6): δ 7.21–6.89 (br, 4H, $\text{H}_{2,6}$), 6.14 (d, $J=8.52$ Hz, 2H, H_4). $^{19}\text{F}\{^1\text{H}\}$ NMR (DMSO- d_6): δ –111.97 (t, $J=8.5$ Hz, $\text{F}_{3,5}$). FT-IR (KBr, cm^{-1}): ν (N–H) 3288.43(m), 3192.34(s), 3114(m), δ (N–H) 1608.00(s), 1572.35(w), 1478.85(m). MS-FAB $^+$: m/z 399 (M^+ – Cl 3%). Elemental analysis for $[\text{C}_{12}\text{H}_{10}\text{F}_4\text{N}_2\text{Cl}_2\text{Pd}]$ calcd. %: C, 33.09; H, 2.31; found C, 34.01; H, 2.38.

2.2.5. Synthesis of *trans*- $[\text{Pd}(\text{Cl})_2(\text{NH}_2\text{C}_6\text{H}_2-2,3,4-\text{F}_3)_2]$ (**5**)

Yellow solid, yield 104 mg (85%), mp 248–250 °C. ^1H NMR (DMSO- d_6): δ 6.95 (m, 2H, H_6), 6.52 (br, 2H, H_5), 5.28 (br, 4H, N–H). $^{19}\text{F}\{^1\text{H}\}$ NMR (DMSO- d_6): δ –153.99 (m, F_4), –157.63 (m, F_2), –163.43 (m, F_3). FT-IR (KBr, cm^{-1}) ν (N–H) 3233.05(w), 3176.06(m), 3105.84(m), δ (N–H) 1575.65(m), 1507.42(s). MS-FAB $^+$: m/z 436 (M^+ – Cl, 3%). Elemental analysis for $[\text{C}_{12}\text{H}_8\text{F}_6\text{N}_2\text{Cl}_2\text{Pd}]$ calcd. %: C, 30.57; H, 1.71; found C, 31.49; H, 1.75.

2.2.6. Synthesis of *trans*- $[\text{Pd}(\text{Cl})_2(\text{NH}_2\text{C}_6\text{H}_2-2,3,6-\text{F}_3)_2]$ (**6**)

Yellow solid, yield 110 mg (90%), mp 255–257 °C. ^1H NMR (DMSO- d_6): δ 6.88 (m, 2H, H_4), 6.50 (m, 2H, H_5). $^{19}\text{F}\{^1\text{H}\}$ NMR (DMSO- d_6): δ –131.60 (m, F_6), –139.92 (m, F_3), –151.85 (m, F_2). FT-IR (KBr, cm^{-1}): ν (N–H) 3186.78(m), 3116.05(m); δ (N–H) 1625.12(w), 1577.57(m), 1515.70(s). MS-FAB $^+$: m/z 436 (M^+ – Cl, 4%). Elemental analysis for

[C₁₂H₈F₆N₂Cl₂Pd] calcd. %: C, 30.57; H, 1.71; found C, 30.11; H, 1.74.

2.2.7. Synthesis of *trans*-[Pd(Cl)₂(NH₂C₆H₂-2,4,5-F₃)₂] (7)

Yellow solid, yield 100 mg (82%), mp 258–260 °C. ¹H NMR (DMSO-*d*₆): δ 7.27 (m, 2H, H₆), 6.72 (m, 2H, H₃), 5.25 (br, 4H, N–H). ¹⁹F{¹H} NMR (DMSO-*d*₆): δ –137.24 (m, F₂), –144.41 (m, F₄) –153.54 (m, F₅). FT-IR (KBr, cm⁻¹): ν (N–H) 3227.79(m), 3175.29(m), 3106.59(m), δ (N–H) 1574.47(m), 1524.81(s). MS-FAB⁺: *m/z* 437 (*M*⁺ – Cl, 3%). Elemental analysis for [C₁₂H₈F₆N₂Cl₂Pd] calcd. %: C, 30.57; H, 1.71; found C, 31.24; H, 1.75.

2.2.8. Synthesis of *trans*-[Pd(Cl)₂(NH₂C₆H₂-2,4,6-F₃)₂] (8)

Yellow solid, yield 107 mg (88%), mp 206–208 °C. ¹H NMR (DMSO-*d*₆): δ 6.98 (t, *J* = 8.25 Hz, H_{3,5}), 5.02 (s, 4H, N–H). ¹⁹F{¹H} NMR (DMSO-*d*₆): δ –127.42 (t, *J* = 8.46 Hz, F₄), –129.37 (d, *J* = 8.46 Hz, F_{2,6}). FT-IR (KBr, cm⁻¹): ν (N–H) 3267.77(w), 3192.82(m), 3120.48(m). δ (N–H) 1624.26(m), 1572.37(w), 1509.27(m), 1459.64(w). MS-FAB⁺: *m/z* 437 (*M*⁺ – Cl, 1.5%). Elemental analysis for [C₁₂H₈F₆N₂Cl₂Pd] calcd. %: C, 30.57; H, 1.71; found C, 30.92; H, 1.73.

2.2.9. Synthesis of *trans*-[Pd(Cl)₂(NH₂C₆F₄-4-H)₂] (9)

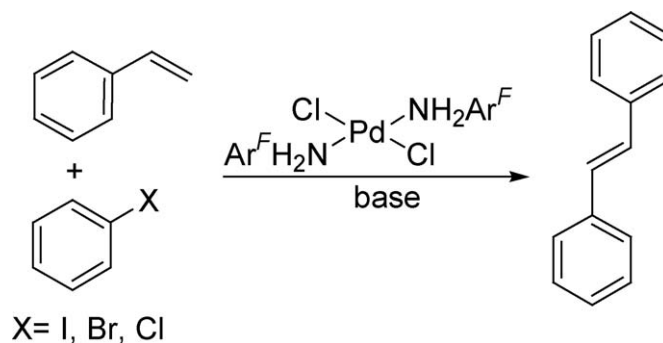
Yellow solid, yield: 72 mg (53%); mp 215–217 °C. ¹H NMR (DMSO-*d*₆): δ = 6.69 (t, *J* = 10.72 Hz, 2H, H₄), 5.91 (br, 4H, N–H). ¹⁹F{¹H} NMR (DMSO-*d*₆): δ –143.03 (m, F_{2,6}), –161.93 (m, F_{3,5}). FT-IR (KBr, cm⁻¹): ν (N–H) 3187.49(m), 3114.41(m); δ (N–H) 1653.16(w), 1577.59(w), 1529.34(s). MS-FAB⁺: *m/z* 507 (*M*⁺, 4%). Elemental analysis for [C₁₂H₆F₈N₂Cl₂Pd] calcd. %: C, 28.40; H, 1.19; Found C, 27.85; H, 1.24.

2.2.10. Synthesis of *trans*-[Pd(Cl)₂(NH₂C₆F₅)₂] (10)

Yellow solid, yield 100 mg (70%), mp 215–217 °C. ¹⁹F{¹H} NMR (DMSO-*d*₆): δ –162.52 (m, F_{2,6}), –166.74 (t, F₄), –178.85 (m, F_{3,5}). FT-IR (KBr, cm⁻¹): ν (N–H) 3189.61(w), 3109.28(w); δ (N–H) 1602.96(m), 1525.09(s). MS-FAB⁺: *m/z* 573 (*M*⁺ – 2Cl, 2%). Elemental analysis for [C₁₂H₄F₁₀N₂Cl₂Pd] calcd. %: C, 26.52; H, 0.74; found: C, 26.73; H, 0.75.

2.3. General procedure for the catalytic reactions

A DMF solution (5 mL) of 50.0 mmol of halobenzene, 60.0 mmol of styrene and the prescribed amount of catalyst was introduced into a Schlenk tube in the open air. The tube was charged with a magnetic stir bar and an equimolar amount of base, sealed and fully immersed in a 160 °C silicon oil bath. After the prescribed reaction time (2 h), the mixture was cooled to room temperature and the organic phase analyzed by gas chromatography (GC–MS) (Scheme 2).



Scheme 2. The palladium catalyzed Heck coupling reaction using *trans*-[PdCl₂(NH₂Ar^F)₂] as catalyst.

2.4. Data collection and refinement for *trans*-[Pd(Cl)₂(NH₂C₆H₃-3,4-F₂)₂] (3), *trans*-[Pd(Cl)₂(NH₂C₆H₃-3,5-F₂)₂] (4) and *trans*-[Pd(Cl)₂(NH₂C₆H₂-2,3,4-F₃)₂] (5)

Crystalline red–orange prisms for **3**, **4** and **5** were grown independently from DMSO (**3**), DMF (**4**) and from a CH₂Cl₂/MeOH solvent system for **5**, and mounted on glass fibers. In all cases, the X-ray intensity data were measured at 293 or 291 K on a Bruker SMART APEX CCD-based X-ray diffractometer system equipped with a Mo-target X-ray tube ($\lambda = 0.71073 \text{ \AA}$). The detector was placed at a distance of 4.837 cm from the crystals in all cases. A total of 1800 frames were collected with a scan width of 0.3° in ω and an exposure time of 10 s/frame. The frames were integrated with the Bruker SAINT software package [5] using a narrow-frame integration algorithm. The integration of the data was done using a monoclinic unit cell in all cases, except for complex **4**, where a triclinic cell was used to yield a total of 15787, 4707 and 6152 reflections for **3**, **4** and **5**, respectively, to a maximum 2θ angle of 50.00° (0.93 Å resolution), of which 4193 (**3**), 2014 (**4**) and 1379 (**5**) were independent. Analysis of the data showed in all cases negligible decays during data collections. The structures were solved by Patterson method using SHELXS-97 [6] program. The remaining atoms were located via a few cycles of least squares refinements and difference Fourier maps, using the space group *C*2(1)/*c* and *P*2(1)/*c* with *Z* = 2 and 4 for **3** and **5**, respectively, and *P*-1 with *Z* = 2 for **4**. Hydrogen atoms were input at calculated positions, and allowed to ride on the atoms to which they are attached. Thermal parameters were refined for hydrogen atoms on the phenyl groups using a $U_{\text{eq}} = 1.2 \text{ \AA}^2$ to precedent atom in all cases. For all complexes, the final cycle of refinement was carried out on all non-zero data using SHELXL-97 [6] and anisotropic thermal parameters for all non-hydrogen atoms. The details of structure determinations are given in Table 1 and selected bond lengths (Å) and angles (°) are given in Tables 2–4, respectively. Numbering of atoms is shown in Figs. 1–3, respectively, (ORTEP) [7].

2.5. Theoretical calculations

Geometry optimizations at the Restricted Hartree–Fock level of theory were carried out using the Gaussian98 suite of

Table 1
Crystal data and structure parameters for *trans*-[Pd(Cl)₂(NH₂C₆H₃-3,4-F₂)₂] (**3**), *trans*-[Pd(Cl)₂(NH₂C₆H₃-3,5-F₂)₂] (**4**) and *trans*-[Pd(Cl)₂(NH₂C₆H₂-2,3,4-F₃)₂] (**5**)

Identification code	3	4	5
Empirical formula	C ₁₆ H ₂₂ Cl ₂ F ₄ N ₂ O ₂ PdS ₂	C ₉ H ₁₂ ClF ₂ N ₂ OPd _{0.5}	C ₆ H ₂ ClF ₃ NPd _{0.5}
Formula weight	591.78	290.86	233.74
Temperature (K)	293(2)	293(2)	291(2)
Wavelength (Å)	0.71073	0.71073	0.71073
Crystal system	Monoclinic	Triclinic	Monoclinic
Space group	C2(1)/c	P-1	P2(1)/c
Unit cell dimensions	$a = 10.763(1) \text{ \AA}$ $\alpha = 90^\circ$ $b = 15.098(1) \text{ \AA}$ $\beta = 94.152(1)^\circ$ $c = 7.1598(4) \text{ \AA}$ $\gamma = 90^\circ$	$a = 5.9282(5) \text{ \AA}$ $\alpha = 94.267(2)^\circ$ $b = 9.0285(8) \text{ \AA}$ $\beta = 99.050(2)^\circ$ $c = 11.057(1) \text{ \AA}$ $\gamma = 98.436(2)^\circ$	$a = 13.0625(8) \text{ \AA}$ $\alpha = 90^\circ$ $b = 7.8514(5) \text{ \AA}$ $\beta = 98.9030(10)^\circ$ $c = 7.7548(5) \text{ \AA}$ $\gamma = 90^\circ$
Volume (Å ³)	1160.4(2)	575.24(9)	785.74(9)
Z	2	2	4
Density (calculated) (Mg/m ³)	1.694	1.679	1.976
Absorption coefficient (mm ⁻¹)	1.256	1.093	1.579
F(0 0 0)	592	292	448
Crystal size	0.316 mm × 0.310 mm × 0.146 mm	0.24 mm × 0.12 mm × 0.07 mm	0.38 mm × 0.35 mm × 0.07 mm
θ range for data collection (°)	1.90–32.55	187–24.98	3.04–24.99
Index ranges	$-16 \leq h \leq 16, -22 \leq k \leq 22, -10 \leq l \leq 10$	$-7 \leq h \leq 7, -10 \leq k \leq 10, -13 \leq l \leq 13$	$-15 \leq h \leq 15, -9 \leq k \leq 9, -9 \leq l \leq 9$
Reflections collected	15787	4707	6152
Independent reflections	4193 [R(int) = 0.0862]	2014 [R(int) = 0.0334]	1379 [R(int) = 0.0292]
Absorption correction	Analytical: face-indexed	Analytical	Integration
Max. and min. transmission	0.8404 and 0.6112	0.9299 and 0.8186	0.8896 and 0.5622
Refinement method	Full-matrix least-squares on F ²	Full-matrix least-squares on F ²	Full-matrix least-squares on F ²
Data/restraints/parameters	4193/0/143	2014/0/150	1379/0/111
Goodness-of-fit on F ²	1.017	0.997	1.001
Final R indices [I > 2 σ (I)]	R1 = 0.0397, wR2 = 0.0840	R1 = 0.0249, wR2 = 0.0527	R1 = 0.0393, wR2 = 0.1097
R indices (all data)	R1 = 0.0552, wR2 = 0.0905	R1 = 0.0262, wR2 = 0.0531	R1 = 0.0427, wR2 = 0.1137
Largest diff. peak and hole	1.023 and -0.434 e\AA^{-3}	0.296 and -0.376 e\AA^{-3}	0.769 and -1.068 e\AA^{-3}

$$R1 = \frac{|F_o - F_c|}{|F_o|}, \quad wR2 = [w((F_o)^2 - (F_c)^2) - w(F_o)^2]^{1/2}.$$

Table 2
Selected bond lengths and angles for *trans*-[Pd(Cl)₂(NH₂C₆H₃-3,4-F₂)₂] (**3**)

Bond lengths (Å)		Angles (°)	
Pd(1)–N(1)	2.0461(19)	N(1)–Pd(1)–N(1)#1	180.00
Pd(1)–N(1)#1	2.0461(19)	N(1)–Pd(1)–Cl(1)	89.92(6)
Pd(1)–Cl(1)	2.2989(6)	N(1)#1–Pd(1)–Cl(1)	90.08(6)
Pd(1)–Cl(1)#1	2.2989(6)	N(1)–Pd(1)–Cl(1)#1	90.08(6)
		N(1)#1–Pd(1)–Cl(1)#1	89.92(6)
		Cl(1)–Pd(1)–Cl(1)#1	180.00

Symmetry transformations used to generate equivalent atoms: #1 $-x, -y, -z + 2$.

Table 3
Selected bond lengths and angles for *trans*-[Pd(Cl)₂(NH₂C₆H₃-3,5-F₂)₂] (**4**)

Bond lengths (Å)		Angles (°)	
Pd(1)–N(1)	2.052(2)	N(1)–Pd(1)–N(1)#1	180.00(1)
Pd(1)–N(1)#1	2.052(2)	N(1)–Pd(1)–Cl(1)	90.30(6)
Pd(1)–Cl(1)	2.3047(6)	N(1)#1–Pd(1)–Cl(1)	89.70(6)
Pd(1)–Cl(1)#1	2.3047(6)	N(1)–Pd(1)–Cl(1)#1	89.70(6)
		N(1)#1–Pd(1)–Cl(1)#1	90.30(6)
		Cl(1)–Pd(1)–Cl(1)#1	180.00

Symmetry transformations used to generate equivalent atoms: #1 $-x + 1, y + 1, -z + 1$.

Table 4
Selected bond lengths and angles for *trans*-[Pd(Cl)₂(NH₂C₆H₂-2,3,4-F₃)₂] (**5**)

Bond lengths (Å)		Angles (°)	
Pd(1)–N(1)	2.052(4)	N(1)–Pd(1)–N(1)#1	180.00
Pd(1)–N(1)#1	2.052(4)	N(1)–Pd(1)–Cl(2)	89.35(13)
Pd(1)–Cl(2)	2.2919(10)	N(1)#1–Pd(1)–Cl(2)	90.65(13)
Pd(1)–Cl(2)#1	2.2919(10)	N(1)–Pd(1)–Cl(2)#1	90.65(13)
		N(1)#1–Pd(1)–Cl(2)#1	89.35(13)
		Cl(2)–Pd(1)–Cl(2)#1	180.00

Symmetry transformations used to generate equivalent atoms: #1 $-x + 1, y + 2, -z$.

programs [8]. For the fluorinated aniline ligands, a 6-311G** basis set was used, whereas for the respective Pd complexes the Effective Core Potential (ECP) approach was employed using the Hay and Wadt ECP's together with their corresponding basis sets [9]. The ECP replaces the core electrons of the second row atoms and heavier by a set of functions and operators that simulate their effect on the valence electrons. This allows for the use of larger computational resources in the description of the valence electronic structure. A Natural Bond Orbital (NBO) analysis [10] was carried out at the optimized structures in order to assess the electron distribution over the molecules.

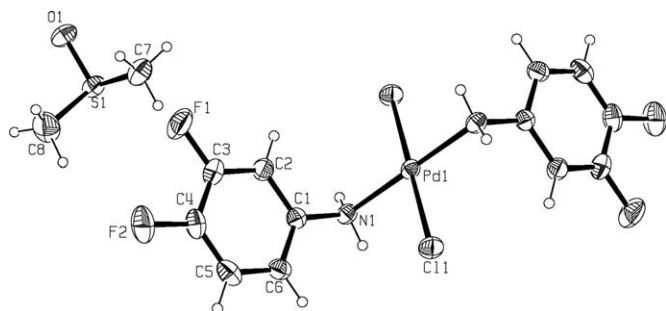


Fig. 1. An ORTEP representation of the structure of *trans*-[Pd(Cl)₂(NH₂C₆H₃-3,4-F₂)₂] (**3**) at 50% probability showing the atom labeling scheme.

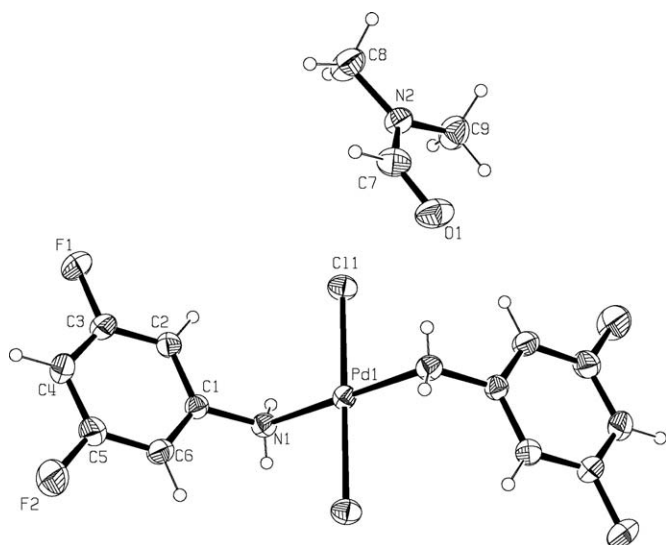


Fig. 2. An ORTEP representation of the structure of *trans*-[Pd(Cl)₂(NH₂C₆H₃-3,5-F₂)₂] (**4**) at 50% probability showing the atom labeling scheme.

In Table 8 the energies for the HOMO in the free aniline ligands are shown. According to the NBO analysis at the optimized geometries the HOMO is constituted by the nitrogen's lone pair (LP) located at the 2p_z Natural Atomic Orbital. This analysis yielded the following relative order of energy for the HOMO:

Disubstituted anilines: **4** < **2** < **1** < **3**.

Trisubstituted anilines: **6** < **7** < **5** < **8**.

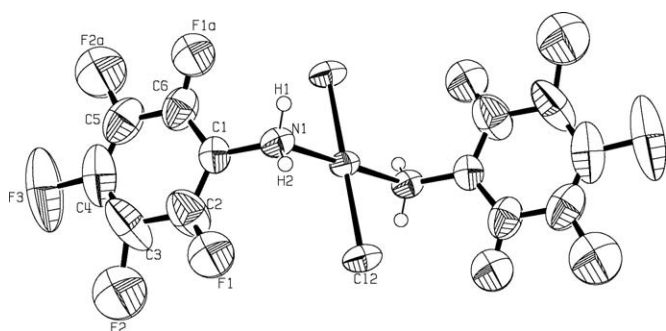


Fig. 3. An ORTEP representation of the structure of *trans*-[Pd(Cl)₂(NH₂C₆H₂-2,3,4-F₃)₂] (**5**) at 50% probability showing the atom labeling scheme.

Table 5
HOMO energies for the free aniline ligands (eV)

Disubstituted anilines		Trisubstituted anilines	
Ligand	E HOMO (eV)	Ligand	E HOMO (eV)
1	−8.5874	5	−8.8582
2	−8.5994	6	−8.9570
3	−8.4985	7	−8.8677
4	−8.6963	8	−8.8337

Molecular conformations optimized with RHF method.

The energy of the LP (HOMO) decreases as its delocalization over the aromatic ring increases. This delocalization of the LP is largely favored by the presence of the electronegative fluorine atoms at *meta*- positions. In the case of the disubstituted anilines it may be observed that the *ortho*- substitution has less influence in the delocalization than the *para*- substitution, since the energy difference for the HOMOs of ligands in **1** and **2** is only slightly higher than 0.01 eV (regardless of the relative *meta*- position in which the second Fluorine atom is located) and the difference between the corresponding values for these ligands and in **3** is approximately 10 times larger (0.1 eV). Having both fluorine atoms at *meta*- positions (ligand in **4**) lowers the energy of the HOMO for the ligand by another 0.1 eV, approximately. A similar trend may be found for the trisubstituted anilines. In the case of ligands in **9** and **10** the values of the energies for the HOMO are −9.3842 and −9.6179 eV, respectively, with a difference of 0.23 eV which exhibits the larger delocalization in ligand in complex **10** by having an extra fluorine atom in *para*- position (Tables 5–7).

The delocalization of the LP over the aromatic ring modifies its availability for coordination to the metallic center, which is

Table 6
Wiberg Pd–N bond index for compounds 1 through 8

Disubstituted anilines		Trisubstituted anilines	
Compound	Pd–N bond index	Compound	Pd–N bond index
1	0.2922	5	0.2957
2	0.2926	6	0.3982
3	0.296	7	0.2918
4	0.2921	8	0.279

Table 7
Wiberg bond indexes for the Pd–Cl bond and the total index for the Pd atom

Compound	Pd–Cl bond index	Total Wiberg bond index for Pd	Pd natural charge
Disubstituted anilines			
1	0.3897	1.434	1.0572
2	0.3905	1.4368	1.0536
3	0.3809	1.4283	1.0612
4	0.383	1.4238	1.062
Trisubstituted anilines			
5	0.3893	1.4409	1.0483
6	0.3982	1.4273	1.0629
7	0.3897	1.4396	1.0504
8	0.3972	1.4318	1.05975

reflected in the Pd–N bond index [11]. As it may be observed in Table 3 the Pd–N bond index becomes higher as the energy of the HOMO of the ligand increases. As the Pd–N bond index increases the Pd–Cl bond index decreases as a mean of preserving the total bond index on the Pd atom. However, these two effects are not mutually compensating and the total Wiberg index for the Pd atom becomes larger as the Pd–N bond index increases. This is also reflected in the natural charge calculated for the Pd atom (see Table 4).

It is possible to notice from Table 8 that the catalytic activity of these complexes increases as the Pd–N bond index increases. According to the Heck's reaction mechanism the first step in the reaction herein studied would be the oxidative addition of bromobenzene to the Pd complex. Thus, the energy of the HOMO in the complexes is the optimal parameter to be analyzed against the conversion yield. It is observed that the complex gets more active towards oxidative addition as the energy of the HOMO in the complex increases and as a consequence the catalytic activity does too.

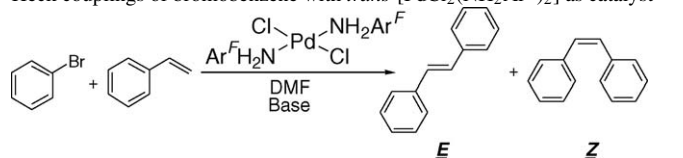
This is directly observed between complexes **9** and **10** in which the presence of an extra fluorine in the *para*- position increases the conversion yield from 41.62 to 51.3%.

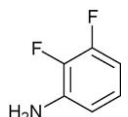
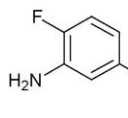
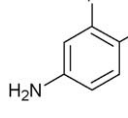
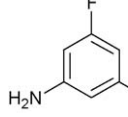
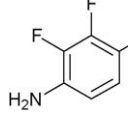
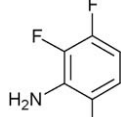
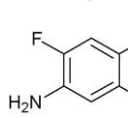
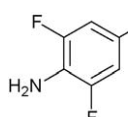
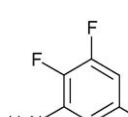
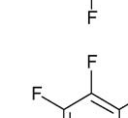
3. Results and discussion

The reaction of two equivalents of the fluorinated anilines with one equivalent of the palladium starting material $[\text{PdCl}_2(\text{C}_6\text{H}_5\text{CN})]$ under reflux afforded in good to excellent yields the complexes $\text{trans}-[\text{PdCl}_2(\text{NH}_2\text{Ar}^F)_2]$ with $\text{Ar}^F = \text{C}_6\text{H}_3\text{-2,3-F}_2$ (**1**), $\text{C}_6\text{H}_3\text{-2,5-F}_2$ (**2**), $\text{C}_6\text{H}_3\text{-3,4-F}_2$ (**3**), $\text{C}_6\text{H}_3\text{-3,5-F}_2$ (**4**), $\text{C}_6\text{H}_2\text{-2,3,4-F}_3$ (**5**), $\text{C}_6\text{H}_2\text{-2,3,6-F}_3$ (**6**), $\text{C}_6\text{H}_2\text{-2,4,5-F}_3$ (**7**), $\text{C}_6\text{H}_2\text{-2,4,6-F}_3$ (**8**), $\text{C}_6\text{F}_4\text{-4-H}$ (**9**), C_6F_5 (**10**), these complexes were characterized by ^1H NMR showing in all cases the presence of the aromatic (except for the case of complex **10**) and N–H protons. More informative results the analyses by ^{19}F NMR where the typical splittings for the presence of the different substitutions in the fluorinated anilines moiety for complexes **1** through **10** are observed [12]. Infrared spectra of these complexes in all cases reveal the N–H stretching and the in-plane deformation frequencies to be located at about 3000 and 1500 cm^{-1} , respectively. Analyses of the aniline compounds by FAB^+ spectrometry affords in most of the cases the molecular ion minus a chloride $[M^+ - \text{Cl}]$, other important peaks include the consecutive lost of chlorides. In all cases elemental analysis are consistent with the proposed formulations.

Crystals suitable for single crystal X-ray diffraction analyses (Table 1) were obtained for complexes **3**, **4** and **5**, being the only difference the fluorinated substituent, the three structures share a number of common features. The palladium centers are located into a square planar environment, having the fluorinated aniline ligands in a *trans* configuration and completing the coordination sphere the two chlorides. Bond lengths and bond angles in all three complexes are comparable to those found in $\text{trans}-[\text{PdCl}_2(\text{H}_2\text{NC}_6\text{H}_4\text{-3-F})_2]$ [13], the largest deviation from the ideal bond angles being observed for complex **5** in $\text{N}(1)\text{-Pd}(1)\text{-Cl}(2)$ [89.35(13)]. It is interesting to notice that while some fluorinated anilines have been extensively used as precur-

Table 8
Heck couplings of bromobenzene with $\text{trans}-[\text{PdCl}_2(\text{NH}_2\text{Ar}^F)_2]$ as catalyst



Entry	NH_2Ar^F	E HOMO (eV)	% Conversion ^a
1		−10.3314	51.45
2		−10.2607	56.30
3		−10.1358	57.48
4		−10.3279	45.20
5		−10.6887	64.33
6		−10.4068	59.10
7		−10.6462	52.32
8		−10.3132	47.48
9			51.3
10			41.62

Reaction conditions 50 mmol of halobenzene, 60 mmol of styrene, 60 mmol of base, 4.0×10^{-5} mmol of catalyst and 5 mL of DMF, 2 h at 160°C .

^a Yields obtained by GC are based on bromobenzene.

sors for the synthesis of Schiff base ligands, crystallographically characterized examples of transition metal complexes containing the bound aniline itself are rare [13,14].

The high melting points that these complexes exhibited (high thermal stability) and the attention that palladium complexes have attracted in the last years in the homogeneous catalysis field prompted us to test their catalytic activity in the catalyzed arylation of haloarenes (Heck reaction). Initial tests carrying out the reaction of iodobenzene with styrene afforded in all cases quantitative yields (6 h reaction time, 160 °C reaction temperature), however more illustrative resulted the catalytic reaction of bromobenzene with styrene, these experiments were carried out under similar reaction conditions (2 h reaction time, 160 °C reaction temperature) with all 10 complexes, resulting complex **5** to be the most reactive. This is curious considering the fact that this results has been previously observed in a different reaction (thiolation) catalyzed by NCN pincer Ni(II) complexes, were the species $[\text{NiCl}_2\{\text{C}_5\text{H}_3\text{N}-2,6-(\text{CHNC}_6\text{H}_2-2,3,4-\text{F}_3)_2\}]$ also resulted to be the more reactive in a similar series of complexes (Scheme 3) [15].

The fact that these complexes are not sensitive to oxygen or water allowed us to carry out all the experiments in the open air using technical grade reagents. Although no clear trend is observed regarding the fluorine content in the different complexes it is clear that the particular substitution pattern of complex **5** favors either more active or more stable species that in turn may favor more the catalytic activity of the corresponding complexes they form.

In order to shed some light in this respect we carried out some theoretical calculations, the results obtained indicate that the fluorinated aniline in complex **5** presents a strong electron withdrawing substituent such that the electronic pair in the nitrogen is less available, this fact may in turn favor the formation of stronger Pd–N bonds. However, a quick analysis of the bond distances of the crystal structures shown in the present paper do not reveal considerable differences in bond distances with respect to the different anilines (complexes **3**, **4** and **5**), however this may also be a consequence of the packing of the different molecules in the solid state. Thus, it seems that there is a subtle balance between the electronics and sterics in the present catalytic system that allows complex **5** to be the more active in the arylation of iodo and bromo benzene with styrene.

Experiments using chlorobenzene resulted only in traces of the products probably as a consequence of the quick and clear decomposition of the complexes in the reaction mixture to palladium black.

There has been a considerable debate in the literature about the oxidation states of the species involved in the catalytic cycle

with Pd(IV)/Pd(II) and Pd(II)/Pd(0) both being proposed at various times [16], however in this case given the type of species involved we favor the Pd(0)/Pd(II) mechanism although the precise mechanism of the catalytic reaction remains to be elucidated.

In conclusion we have reported a high yield procedure for the synthesis of fluorinated aniline-palladium complexes of the type $\text{trans}-[\text{PdCl}_2(\text{NH}_2\text{Ar}^F)_2]$, these compounds efficiently catalyzed the Heck reaction of iodo and bromo benzene with styrene in the complete absence of phosphines. It is noteworthy that the attractive features of this catalytic system of good yields and air and water stability and easiness for the synthesis of the catalytic precursors approach those required for commercial viability and opens future possibilities for its use in other palladium catalyzed reactions, this research is currently under investigation.

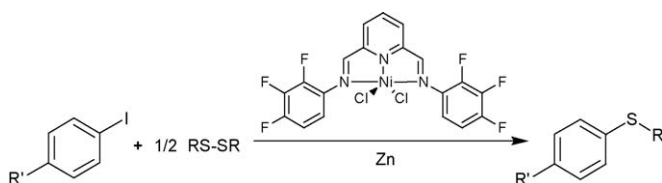
Moreover, from the theoretical calculations the following general principles may be observed, even when it is not possible to obtain a strict relationship between the substitution pattern on the ligand and the conversion. The catalytic activity tends to increase as the energy of the HOMO increases. This in turn increases with electron donation from the ligand to the metallic center (this feature assessed by the Pd–N Wiberg bond index). This electron donation becomes larger as the lone pair from the N atom in the ligand is less delocalized over the aromatic ring. In order to prevent delocalization of the lone pair, and therefore increase the Pd–N bond index in the complex, substitution of the *meta*- positions with fluorine atoms, over the *ortho*- and *para*-, will render the desired effect. Thus, from the present data it seems that substitution of the *meta*- positions by a stronger electron donor substituent would decrease even more the delocalization of the LP and this in turn would tend to increase the yield in the catalytic transformation by an increase of the energy of the HOMO in the Pd complex, activating it for the first step of oxidative addition in the Heck reaction, these modifications are currently under investigation.

Supplementary material

Supplementary data for complexes **3**, **4** and **5** have been deposited at the Cambridge Crystallographic Data Centre. Copies of this information are available free of charge on request from The Director, CCDC, 12 Union Road, Cambridge CB2 1EZ, UK (Fax: +44 1223 336033; e-mail: deposit@ccdc.cam.ac.uk or [www: http://www.ccdc.cam.ac.uk](http://www.ccdc.cam.ac.uk)) quoting the deposition numbers CCDC 281879 (**3**), CCDC 281878 (**4**) and CCDC 281880 (**5**).

Acknowledgements

O. B.-P and J. B.-F would like to thank CONACYT for financial support. We would like to thank Chem. Eng. Luis Velasco Ibarra and M.Sc. Francisco Javier Pérez Flores, QFB. Ma del Rocío Patiño and Ma de las Nieves Zavala for their invaluable help in the running of the FAB⁺-Mass, IR and ¹⁹F{¹H} spectra, respectively. The support of this research by CONACYT (J41206-Q) and DGAPA-UNAM (IN114605) is gratefully acknowledged. We would like to thank DGSCA for generous



Scheme 3.

allocation of CPU time in the ORIGIN 2000 supercomputer. Special thanks to David Vázquez for keeping running the network at the Instituto de Química-UNAM. We would like to thank Prof. Keith Hollis for careful proof reading of the manuscript.

References

- [1] B. Cornils, W.A. Herrmann (Eds.), *Applied Homogeneous Catalysis with Organometallic Compounds*, vol. 2, Wiley-VCH Verlag GmbH, Federal Republic of Germany, 2002 (Chapter 3).
- [2] A.M. Rouhi, *Chem. Eng. News*. 82 (2004) 49.
- [3] (a) D. Morales-Morales, R. Redón, Y. Zheng, J.R. Dilworth, *Inorg. Chim. Acta*. 328 (2002) 39;
(b) D. Morales-Morales, C. Grause, K. Kasaoka, R. Redón, R.E. Cramer, C.M. Jensen, *Inorg. Chim. Acta*. 300–302 (2000) 958;
(c) D. Morales-Morales, R. Redón, Z. Wang, D.W. Lee, C. Yung, K. Magnuson, C.M. Jensen, *Can. J. Chem.* 79 (2001) 823;
(d) D. Morales-Morales, R.E. Cramer, C.M. Jensen, *J. Organomet. Chem.* 654 (2002) 44;
(e) X. Gu, W. Chen, D. Morales-Morales, C.M. Jensen, *J. Mol. Catal. A* 189 (2002) 119;
(f) J.R. Dilworth, P. Arnold, D. Morales, Y.L. Wong, Y. Zheng, *The chemistry and applications of complexes with sulphur ligands*, in: *Modern Coordination Chemistry. The Legacy of Joseph Chatt*, Royal Society of Chemistry, Cambridge, UK, 2002, p. 217;
(g) D. Morales-Morales, R. Redón, C. Yung, C.M. Jensen, *Inorg. Chim. Acta*. 357 (2004) 2953;
(h) C. Herrera-Álvarez, V. Gómez-Benítez, R. Redón, J. García-Alejandre, S. Hernández-Ortega, R.A. Toscano, D. Morales-Morales, *J. Organomet. Chem.* 689 (2004) 2464;
(i) G. Ríos-Moreno, R.A. Toscano, R. Redón, H. Nakano, Y. Okuyama, D. Morales-Morales, *Inorg. Chim. Acta*. 358 (2005) 303;
(j) J.G. Fierro-Arias, R. Redón, J. García-Alejandre, S. Hernández-Ortega, R.A. Toscano, D. Morales-Morales, *J. Mol. Catal. A* 233 (2005) 17.
- [4] G.K. Anderson, M. Lin, *Inorg. Synth.* 28 (1990) 60.
- [5] Bruker AXS, *SAINT Software Reference Manual*, Madison, WI, 1998.
- [6] G.M. Sheldrick, *SHELXTL NT Version 6.10*, Program for Solution and Refinement of Crystal Structures, University of Göttingen, Germany, 2000.
- [7] L.J. Farrugia, *J. Appl. Cryst.* 30 (1997) 565.
- [8] M.J. Frisch, G.W. Trucks, H.B. Schlegel, G.E. Scuseria, M.A. Robb, J.R. Cheeseman, V.G. Zakrzewski, J.A. Montgomery Jr., R.E. Stratmann, J.C. Burant, S. Dapprich, J.M. Millam, A.D. Daniels, K.N. Kudin, M.C. Strain, O. Farkas, J. Tomasi, V. Barone, M. Cossi, R. Cammi, B. Mennucci, C. Pomelli, C. Adamo, S. Clifford, J. Ochterski, G.A. Petersson, P.Y. Ayala, Q. Cui, K. Morokuma, N. Rega, P. Salvador, J.J. Dannenberg, D.K. Malick, A.D. Rabuck, K. Raghavachari, J.B. Foresman, J. Cioslowski, J.V. Ortiz, A.G. Baboul, B.B. Stefanov, G. Liu, A. Liashenko, P. Piskorz, I. Komaromi, R. Gomperts, R.L. Martin, D.J. Fox, T. Keith, M.A. Al-Laham, C.Y. Peng, A. Nanayakkara, M. Challacombe, P.M.W. Gill, B. Johnson, W. Chen, M.W. Wong, J.L. Andres, C. Gonzalez, M. Head-Gordon, E.S. Replogle, J.A. Pople, *Gaussian98 Revision A.11.3*, Gaussian, Inc., Pittsburgh, PA, 2002.
- [9] (a) P.J. Hay, W.R. Wadt, *J. Chem. Phys.* 82 (1985) 270;
(b) W.R. Wadt, P.J. Hay, *J. Chem. Phys.* 82 (1985) 284;
(c) P.J. Hay, W.R. Wadt, *J. Chem. Phys.* 82 (1985) 299.
- [10] E.D. Glendening, A.E. Reed, J.E. Carpenter, F. Weinhold, *NBO Version 3.1*.
- [11] K.B. Wiberg, *Tetrahedron* 24 (1968) 1083.
- [12] M.E. Peach, *Can. J. Chem.* 46 (1968) 2699.
- [13] V.M. Padmanabhan, R.P. Patel, T.N. Ranganathan, *Acta Cryst.* C41 (1985) 1305.
- [14] J. Fawcett, F. Sicilia, G.A. Solan, *Acta Cryst.* E61 (2005) m1256.
- [15] (a) O. Baldovino-Pantaleón, S. Hernández-Ortega, D. Morales-Morales, *Inorg. Chem. Commun.* 8 (2005) 955;
(b) O. Baldovino-Pantaleón, S. Hernández-Ortega, D. Morales-Morales, *Adv. Synth. Catal.*, in press.
- [16] (a) D. Morales-Morales, R. Redón, C. Yung, C.M. Jensen, *Chem. Commun.* (2000) 1619;
(b) I.P. Beletskaya, A.V. Cheprakov, *Chem. Rev.* 100 (2000) 3009.